Manuscript submitted to:

AIMS Energy

Volume 3, Issue 2, 172-182

DOI:10.3934/energy.2014.2.172

Received 16 January 2014, Accepted 3 April 2014, Published 30 April 2014

Research Article

Pressurized Carbon Dioxide as Heat Transfer Fluid: Influence of Radiation on Turbulent Flow Characteristics in Pipe

Cyril Caliot[1] **Gilles Flamant**[1*]

[1] Processes, Materials, and Solar Energy Laboratory, PROMES-CNRS,Centre F. Trombe, 7 Rue du Four Solaire,66120 Font-Romeu-Odeillo, France

[*] **Correspondence:** Gilles.Flamant@promes.cnrs.fr

Abstract: The influence of radiative heat transfer in a CO_2 pipe flow is numerically investigated at different pressures. Coupled heat and mass transfer, including radiation transport, are modeled. The physical models and the high temperature and high pressure radiative properties method of computation are presented. Simulations are conducted for pure CO_2 flows in a high temperature pipe at 1100 K (with radius 2 cm) with a fixed velocity (1 $m.s^{-1}$) and for different operating pressures, 0.1, 1, 5 and 20 MPa (supercritical CO_2). The coupling between the temperature and velocity fields is discussed and it is found that the influence of radiation absorption is important at low pressure and as the operating pressure increases above 5 MPa the influence of radiation becomes weaker due to an increase of CO_2 optical thickness.

Keywords: Radiation transport, CO2 radiative properties, high pressure carbondioxide spectra, computational fluid dynamics, supercritical carbon dioxide flow, radiation andflow coupling

1. Introduction

Current heat transfer fluids (HTF) for solar concentrating systems are: synthetic oil, steam, molten salt and air. At temperature higher than 565 °C air is the only available HTF, but the poor heat transfer properties of air are well known. Consequently, researches on alternative HTF for the conversion of concentrated solar energy at high temperature (high Carnot efficiency) is an important R&D topic for improving actual technologies. A review of thermodynamic cycles and working fluid has been published in [1] but for low-grade heat. Carbon dioxide appears to be a good candidate because it is non-flammable and non-toxic fluid. The CO_2 supercritical state (s-CO_2) is observed at 73.8 b and 304.5 K consequently favorable heat transfer and viscous supercritical properties may be built on designing innovative conversion systems. Some works have been done in the field of low and medium temperature solar heat conversion. For example, solar-driven carbon dioxide transcritical power system using evacuated tube type solar collectors was studied in [2] whereas supercritical Rankine cycle was examined in [3] and demonstrated in [4]. In this latter paper evacuated CO_2-based solar collectors showed 65-70% solar heat collection efficiency and the measured power conversion efficiency was in the range 8.78-9.45%. At high temperature, it was pointed out in [5] that s-CO_2 recompression Brayton cycle can be as efficient as helium Brayton cycle with lower inlet turbine temperature (550 °C for s-CO_2 vs. 850 °C for He) but higher inlet pressure (20 MPa for s-CO_2 vs 8 MPa for He). In addition, its high working pressure makes the installation more compact and reduces the investment cost. Due to the relatively low inlet turbine temperature, this cycle was mainly studied for power generation in nuclear power plants [5, 6, 7]. However, high temperature s-CO_2 cycles may be used to produce power from concentrated solar energy systems. A molten salt solar tower using s-CO_2 Brayton cycle to produce electricity was described in [8] and the integration of heat storage to a supercritical

CO_2 cycle was presented in [9]. The great potential of advanced s-CO_2 power cycles for concentrated solar energy conversion was demonstrated in [10]. It is shown that cycle configurations such as recompression cycles combined with intercooling and/or turbine reheat are able to achieve efficiency higher than 50% for turbine inlet temperature larger than 700 °C. Concerning heat transfer characteristics, experimental investigation of heat transfer in tubes have been carried out by [11] and [12] using 18.4 mm and 4.4 mm i.d. tubes respectively with s-CO_2 at pressures slightly higher than the supercritical one. Fully developed turbulent flow was studied in [12]. This overview of published works indicates the great potential of s-CO_2 for the conversion of concentrated solar energy but that radiation effect on heat exchange performances have been neglected although carbon dioxide is a well known absorbing gas in the IR region. Consequently, the objective of the present article is to show the influence of radiation in a pure CO_2 turbulent pipe flow as a function of pressure. A numerical approach is used to simulate the flow and heat transfer accounting for radiation transport since the pipe wall is at high temperature and CO_2 participates in radiation. First, the model is presented, then the simulation is described and, finally, the results are discussed in the last section.

2. Mathematical models

2.1. Mass transfer model

The mass balance equation and the momentum balance equation for the turbulent flow are solved. The turbulent flow is modeled with a steady Reynolds-averaged Navier-Stokes model which is the standard k-epsilon model. Therefore, the flow dynamics is modelled using the following steady state balance equations for mass (Eq. 1) and momentum (Eq. 2):

$$\frac{\partial}{\partial x_i}(\rho u_i) = 0 \tag{1}$$

$$\begin{aligned}\frac{\partial}{\partial x_j}(\rho u_i u_j) = &- \frac{\partial p}{\partial x_i} + \frac{\partial}{\partial x_j}\left[\mu\left(\frac{\partial u_i}{\partial x_j} + \frac{\partial u_j}{\partial x_i} - \frac{2}{3}\delta_{ij}\frac{\partial u_l}{\partial x_l}\right)\right] \\ &+ \frac{\partial}{\partial x_j}\left[\left(\mu_t\left(\frac{\partial u_i}{\partial x_j} + \frac{\partial u_j}{\partial x_i}\right) - \frac{2}{3}\left(\rho k + \mu_t\frac{\partial u_k}{\partial x_k}\right)\delta_{ij}\right]\end{aligned} \tag{2}$$

where velocity u_i and pressure p are Favre's mean variables (mass-averaged values) and where the Boussinesq approach is used to model the Reynolds stresses. The turbulent viscosity μ_t is modeled by a $k-\epsilon$ approach, therefore it depends on the turbulent kinetic energy k and its dissipation rate ϵ following the relationship $\mu_t = \rho C_\mu \frac{k^2}{\epsilon}$. Thus, two additional equations for k and ϵ are solved:

$$\frac{\partial}{\partial t}(\rho k) + \frac{\partial}{\partial x_i}(\rho k u_i) = \frac{\partial}{\partial x_j}\left[\left(\mu + \frac{\mu_t}{\sigma_k}\right)\frac{\partial k}{\partial x_j}\right] + \mu_t 2 S_{ij} S_{ij} - \rho\epsilon \tag{3}$$

$$\frac{\partial}{\partial t}(\rho \epsilon) + \frac{\partial}{\partial x_i}(\rho \epsilon u_i) = \frac{\partial}{\partial x_j}\left[\left(\mu + \frac{\mu_t}{\sigma_\epsilon}\right)\frac{\partial \epsilon}{\partial x_j}\right] + C_{1\epsilon}\frac{\epsilon}{k}\mu_t 2 S_{ij} S_{ij} - C_{2\epsilon}\rho\frac{\epsilon^2}{k} \tag{4}$$

where the following constants are used: $C_{1\epsilon} = 1.44$, $C_{2\epsilon} = 1.92$, $C_\mu = 0.09$, $\sigma_k = 1.0$, $\sigma_\epsilon = 1.3$; and S_{ij} represents the mean rate-of-strain tensor.

The density, specific heat capacity, thermal conductivity and viscosity of CO_2 were extracted from the work of [13].

2.2. Heat transfer model

Turbulent heat transport is modeled using the concept of Reynolds' analogy to turbulent momentum transfer. The energy balance equation is thus given by:

$$\frac{\partial}{\partial t}(\rho E) + \frac{\partial}{\partial x_i}[u_i(\rho E + p)] = \frac{\partial}{\partial x_j}\left(\lambda_{\text{eff}}\frac{\partial T}{\partial x_j} + u_i\mu_t\left(\frac{\partial u_j}{\partial x_i} + \frac{\partial u_i}{\partial x_j}\right) - u_i\frac{2}{3}\mu_t\frac{\partial u_k}{\partial x_k}\delta_{ij}\right) + S_{\text{rad}} \tag{5}$$

where E is the total energy and λ_{eff} is the effective thermal conductivity, $\lambda_{\text{eff}} = \lambda + \frac{c_p\mu_t}{\text{Pr}_t}$ (with λ the thermal conductivity and $\text{Pr}_t = 0.85$).

The energy balance equation includes a radiative source term, S_{rad}, to account for CO_2 participation in radiation transport inside the pipe. Indeed, carbon dioxide is a participating medium that strongly absorbs infrared radiation mainly in the 2.7 μm bands, 4.3 μm bands and 15 μm bands. Carbone dioxide is a semi-transparent gas that emits radiation and mainly absorbs radiation emitted from the high temperature pipe wall. Thus, radiation absorption can play a significant role in heat transfer balance.

2.3. Radiative transfer model

Radiation transport is considered in an emitting, absorbing, non-scattering and non-gray medium surrounded by gray walls. The monochromatic RTE (Radiative Transfer Equation) for an absorbing and emitting medium, at position $\vec{r}$ and in the direction $\vec{s}$, can be written as:

$$\frac{\text{d}I_\nu}{\text{d}s} = \kappa_\nu(I_{b\nu} - I_\nu) \tag{6}$$

with the associated boundary condition for a gray surface that emits and reflects diffusely:

$$I_{w\nu}(\vec{s}) = \epsilon_w I_{b\nu} + \frac{1-\epsilon_w}{\pi}\int_{\vec{n}\cdot\vec{s'}<0} |\vec{n}\cdot\vec{s'}| I_\nu(\vec{s'})\text{d}\Omega' \tag{7}$$

The radiative property model chosen in this study is a multi-gray approach and the RTE for the jth gray component is expressed as [14]:

$$\frac{\text{d}I_j}{\text{d}s} = \kappa_j(a_j\frac{\sigma T^4}{\pi} - I_j) \tag{8}$$

where a_j and κ_j are, respectively, the emission weighting factor and absorption coefficient for the jth gray component. The quantities a_j and κ_j are temperature dependent. The boundary conditions for gray walls thus become:

$$I_w(\vec{s}) = \epsilon_w a_j\frac{\sigma T^4}{\pi} + \frac{1-\epsilon_w}{\pi}\int_{\vec{n}\cdot\vec{s'}<0} |\vec{n}\cdot\vec{s'}| I_j(\vec{s'})\text{d}\Omega' \tag{9}$$

The radiative source term (in Eq. 5) is computed with a finite volume model for spatial and directional integrations. The radiative transfer equation (Eq. 8) is solved using the Discrete Ordinates (DO) radiation model (as it is called in the ANSYS Fluent commercial software) for a finite number of discrete angles. This DO model corresponds to the finite-volume method developed by Chui and Raithby [15] which is different but presents many similarities with the classical discrete ordinate method. In two-dimensional simulations, only four octants are solved due to symmetry. In the presented two-dimensional simulations, 16 directions are adopted for the angular discretization of each octant. For spectral integration the global spectral ADF (Absorption Distribution Function) model [16] is chosen for the description of global radiative properties of CO_2 at high temperature (ADF-CO_2). These two models (DO and ADF) are approximate models but they are suitable for coupled CFD simulations and do not involve huge computer time.

2.4. Radiative properties of carbon dioxide

The participating medium is pure carbon dioxide at high temperature (up to 1100 K) and from low (0.1 MPa) to high pressure (20 MPa). Therefore, the radiative properties of CO_2 should be computed over a large temperature and pressure ranges. At high temperature, the radiative properties of CO_2 can be computed based on high temperature spectroscopic databases such as HITEMP-2010 [17] or CDSD-4000 [18]. The spectroscopic database selected is HITEMP-2010 because CO_2 temperature does not reach $4000K$ in the present calculation so we do not need to involve transitions occuring around 4000 K. For low pressure, CO_2 spectra can be computed within the limits of the impact approximation based on the isolated line concept. The line shape is considered Lorentzian and accordingly to the isolated line concept, each line shape is not modified by other transitions. However, as pressure increases the gas density increases and the collision-induced transfers of population become important [19]. Spectral transitions can overlap significantly with each other and the isolated line assumption breaks down. Thus, the spectral shape should be modeled with the line mixing process. A line-by-line model [20] was used to obtain synthetic spectra of pure CO_2 assuming a Lorentz line profile corrected by a χ factor [21] that accounts for line mixing effects and results in a transfer of population from line wings to line core. Carbon dioxide spectra were computed for different pressures and temperatures. To ensure short computation time while keeping a sufficient accuracy on the radiative source term computation, the high resolution CO_2 radiative properties should be approximated by a global spectral model requiring only a few number of parameters. Indeed, high resolution spectra requires to discretize absorption coefficient spectra with tens of millions of points whereas a global spectral model requires only few tens of points. High resolution spectra are also necessary to compute the parameters of approximate global spectral models. In this study, spectra were used to create a set of radiative properties based on the Absorption Distribution Function (ADF) global spectral model. The parameters of the ADF-CO_2 model are the gray gases absorption coefficients $k_j(T)$ and its correponding wheights $a_j(T)$. It is assumed that radiation transport in the simulated CO_2 pipe flow is well described using nine grey gases. These parameters were computed after rearranging the global high resolution spectra into k-distributions [16]. The ADF spectral radiative properties of CO_2 were computed based on the high temperature spectroscopic data of HIPTEMP-2010 for CO_2 in the spectral range between 330 and 10000 cm^{-1} (1-30μm). Four sets of ADF-CO_2 parametres were computed for different working pressures (0.1 MPa, 1 MPa, 5 MPa and 20 MPa) and each set of ADF-CO_2 parameters is valid for the temperature range $300 - 1500K$.

As an illustration of carbon dioxide radiative properties, Figure 1 presents an example of its pressure and temperature dependencies. Figure 1(a) shows the evolution of narrow band absorption coefficent spectra for different CO_2 pressures at a temperature of 600 K and Figure 1(b) shows high resolution spectra of CO_2 absorption coefficients (at 0.1 MPa) for two temperatures. At high pressure the absorption coefficient reaches high values and becomes opaque in the band center (Fig. 1)(a). At a pressure of 0.1 MPa the average absorption coefficient is almost superimposed on the x-axis. The temperature dependence of the CO_2 spectra is shown in Fig. 1(b). The absorption coefficient of cold lines decreases when the temperature increases. In addition, towards high wavelength (not shown in Fig. 1(b)), hot lines appear when the temperature increases resulting in a slight increase of the absorption coefficient.

3. Computational implementation of the model

3.1. Numerical methods

The ANSYS Fluent commercial finite volume fluid dynamics solver is used to solve the transport Eqs. (1)-(5) and (8). In particular, the pressure based solver is used, employing the SIMPLE pressure velocity coupling method [22]. Gradients are computed using the least squares cell based method, and the standard pressure

1.pdf

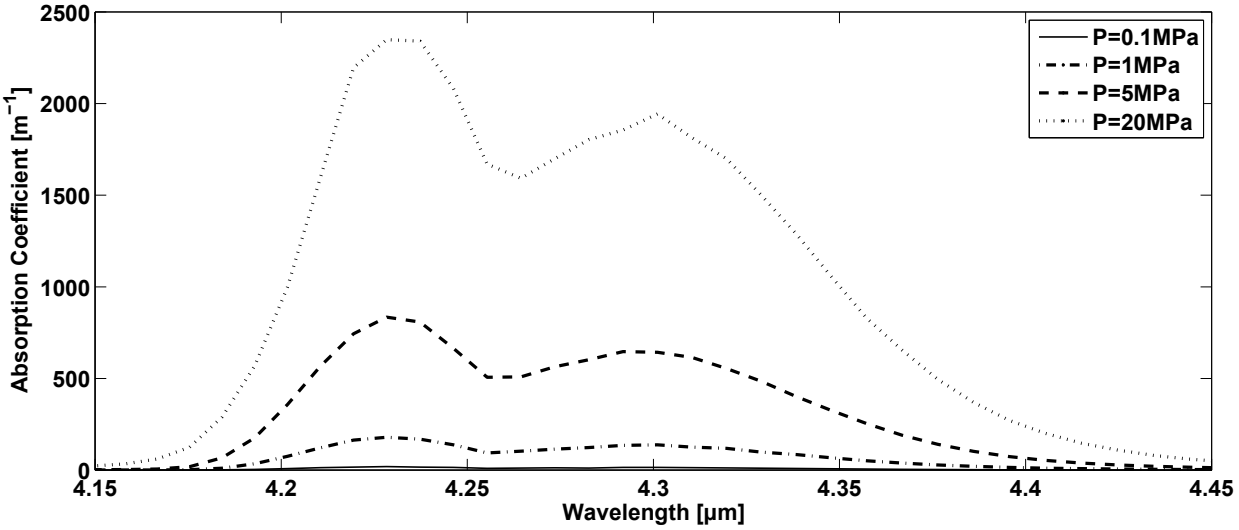

(a) Narrow band absorption coefficient at T = 600 K

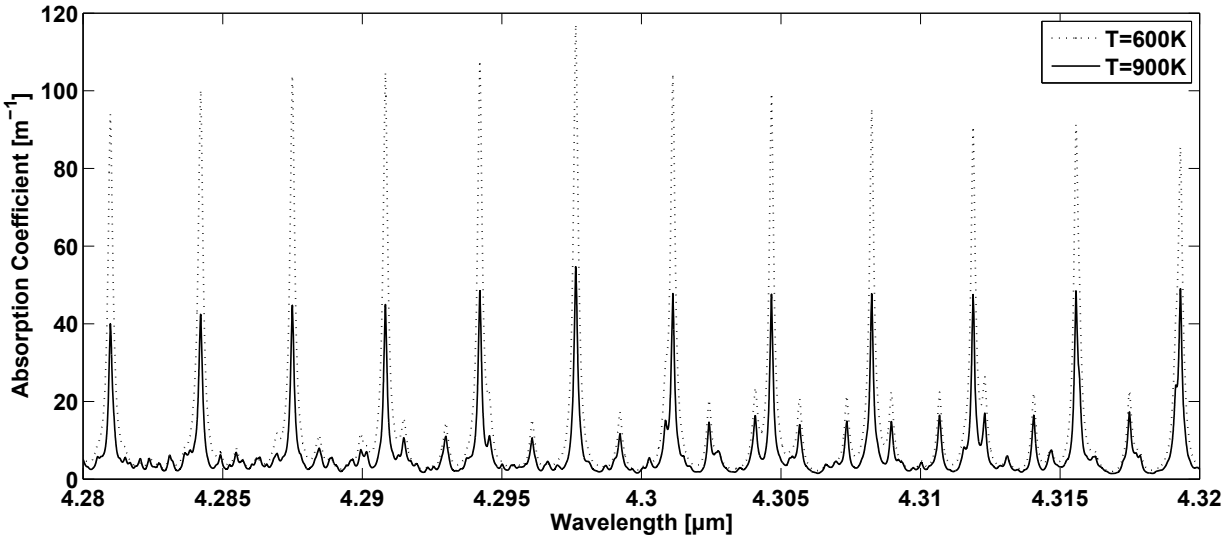

(b) High resolution κ_ν at P = 0.1 MPa

Figure 1. Dependence of gaseous CO_2 absorption coefficient with (a) pressure and (b) temperature

interpolation scheme is used. The QUICK [23] scheme is used for the spatial discretization of the flow and energy transport equations. The near-wall modeling method selected for the wall-bounded turbulent flow is the enhanced-wall-treatment that can be used with fine and coarse meshes [24]. The finite volume method is also employed for the computation of radiation transport using a 4×4 discretization of the zenith and azimuth angles in each octant. The temperature and composition dependent thermo-physical properties of CO_2 are computed for each cell using Fluent's User-Defined-Functions (UDFs). The radiation absorption coefficient is also computed by an UDF. The solution time is several hours (about 10 hours) on a modern PC workstation (parallel Fluent on a Quad Core processor at 2.93 GHz).

4. Results and discussion

4.1. Computational domain

The pipe is circular in cross section and is modelled using a structured two-dimensional axisymmetric grid. The grid is oriented such that the x-direction lies along the length of the reactor and the y-direction lies along the radius of the reactor. The radius and length of the reactor are, respectively, 2 cm and 2 m, leading to an aspect ratio $L/R = 100$.

In the y direction, a refined grid (boundary layer) is used close to the wall, starting with $\Delta y = 10^{-5}$ m and increasing with a growth factor of 1.05 over the first 50 cells. A constant grid spacing of $\Delta y = 2 \times 10^{-4}$ m is used thereafter up to the axis of symmetry. In the x-direction, a grid spacing $\Delta x = 0.5$ mm is used in the refined boundary layer and another grid spacing $\Delta x = 1$ mm is used for the remaining mesh. The total number of cells in the domain is 3.5×10^5. Although not discussed in detail, a grid sensitivity study was performed prior to selecting the present discretization.

4.2. Boundary conditions

The inlet boundary condition is an inlet velocity for pure CO_2 at 400 K and different simulations are conducted with different inlet pressures. The selected pressures cover the range from 0.1 MPa to 20 MPa with intermediate values of 1 MPa and 5 MPa. Similar inlet velocities were chosen for the different flow simulations having different static pressures. The inlet velocity is specified parabolic with a mean value of 1 m/s that leads to 0.0017 kg/s at 0.1 MPa, 0.0169 kg/s at 1 MPa, 0.0915 kg/s at 5 MPa and 0.4782 kg/s at 20 MPa. The flow is heated by the hot pipe wall at a constant temperature of 1100 K considered as a blackbody ($\epsilon_w = 1$).

2.pdf

Figure 2. Sketch of the pipe: axisymmetric temperature field in the simulated CO_2 pipe flow with a real length to radius ratio (T ranging from 300 K, blue, to 1100 K, red).

5. Results and Discussion

A sketch of the reactor is depicted in Figure 2 with a real length to radius ratio. The reactor size does not allow one to clearly represent fields inside the pipe while keeping the real length to radius ratio. This is the reason why the simulated fields inside the reactor will be represented in figures where the radius scale (y axis) is enlarged. The simulation results are presented below in Figures 3 and 4, and the effects of radiation transport

in the pipe are discussed. The fields are depicted using isocontour plots of approximately unit aspect ratio; however, the aspect ratio of the reactor (length to radius ratio) is 100, and, therefore, to correctly interpret the geometry of the intercontour regions it is necessary to consider that the axial distance between contours is 100 times greater than depicted, while gradients with even a small apparent radial component are essentially radial. Concerning the calculated results, the flow and energy conservation were checked numerically between the inlet and the outlet and this step is not shown here.

3.pdf

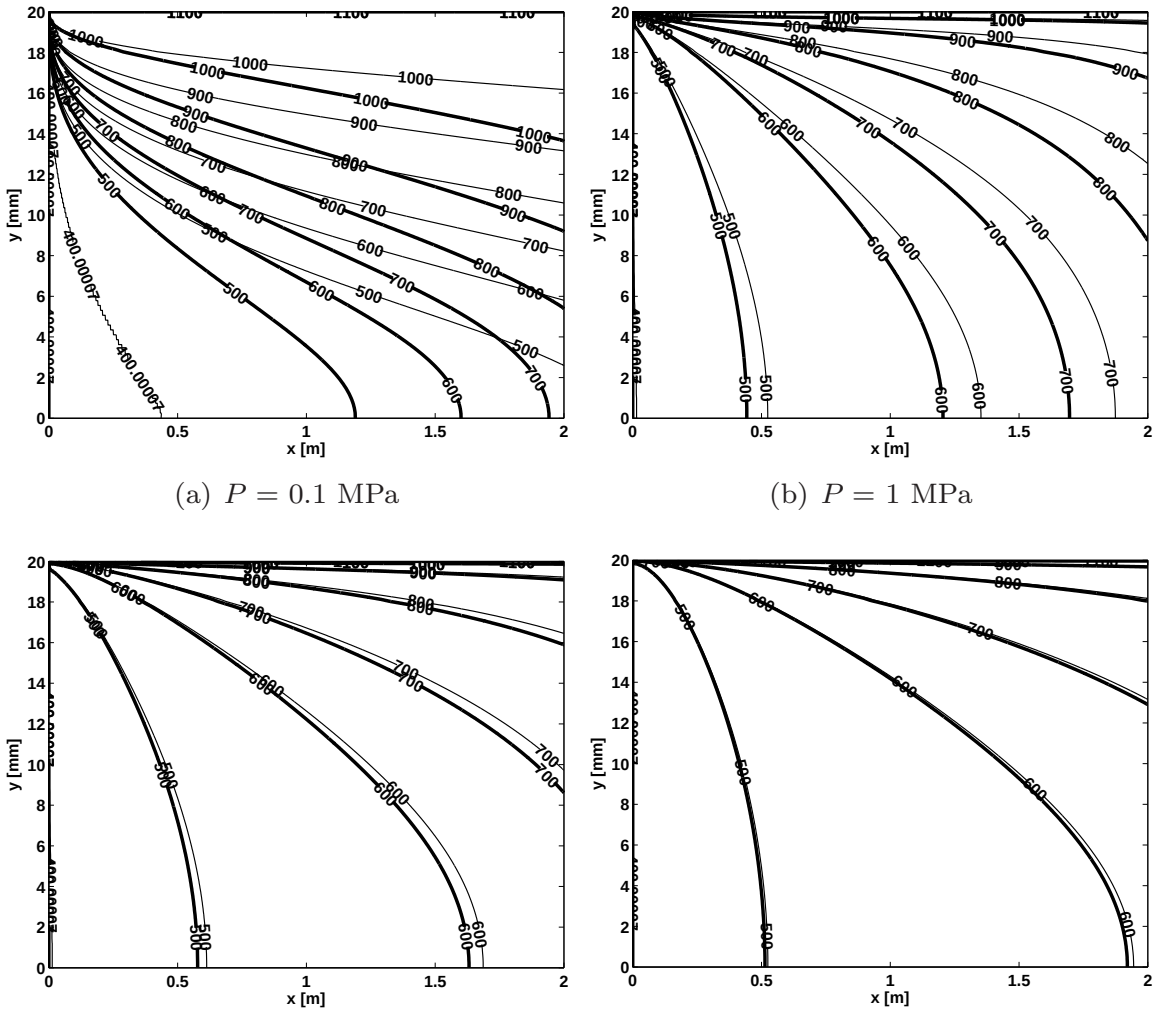

(a) $P = 0.1$ MPa (b) $P = 1$ MPa

(c) $P = 5$ MPa (d) $P = 20$ MPa

Figure 3. Isocontours of temperature in the pipe for simulations with different operating pressures and having all a CO_2 inlet velocity of 1 m/s: the thin solid lines represent fields computed neglecting radiation whereas thick solid line are for fields obtained with the radiation model

The influence of radiation transport on temperature and velocity fields is studied for CO_2 pipe flow at four different pressures. The effect of radiation is highlighted when comparing two simulation results obtained with and without the radiative heat transfer model. Figures 3(a)-3(d) present isocontours of temperature in the axisymmetric geometry of the pipe and Figures 4(a)-4(d) present isocontours of velocity. Because the pipe wall

4.pdf

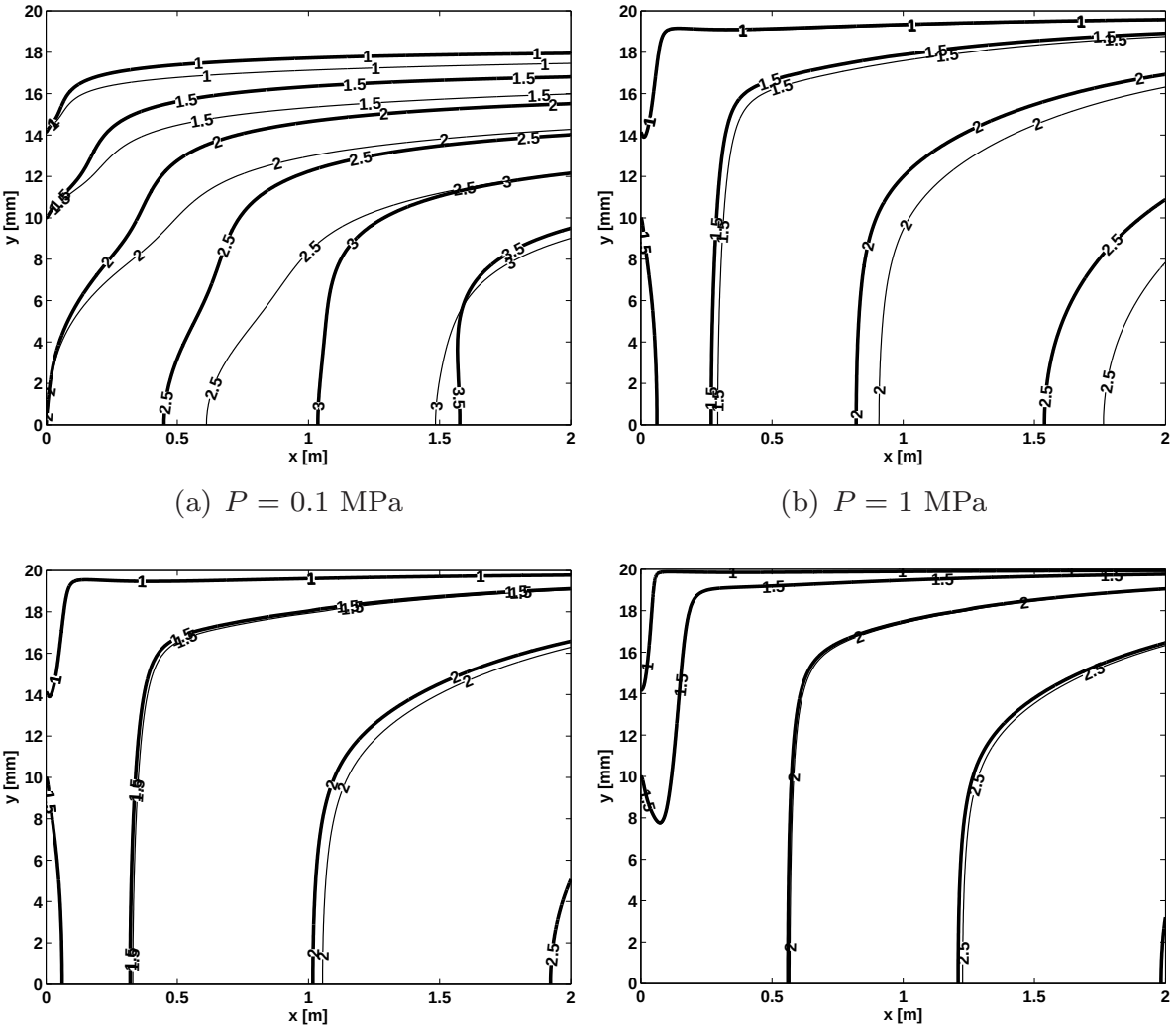

(a) $P = 0.1$ MPa

(b) $P = 1$ MPa

(c) $P = 5$ MPa

(d) $P = 20$ MPa

Figure 4. Isocontours of velocity in the pipe for simulations with different operating pressures and having all a CO_2 inlet velocity of $1\ m/s$: the thin solid lines represent fields computed neglecting radiation whereas thick solid line are for fields obtained with the radiation model

is at high temperature, one can expect that radiation absorption by the CO_2 flow leads to a fluid temperature increase. This phenomena occurs clearly for flows with 0.1 and 1 MPa (Figs 3(a)-3)(b) but tends to diminish for higher pressures (Figs 3(c)-3(d)). Indeed, when comparing the temperature profiles obtained for different pressures and neglecting or not the radiation transport, the results show a decrease of the influence of radiation with respect to a pressure increase. The cross comparison of velocity and temperature fields (Figs 3-4) show also the effect of heat and flow coupling which leads to an acceleration of the flow as the temperature increases (for the same fixed pressure). Consequently, the lower velocity is find for the cases where the influence of radiation absorption is weaker, i.e. at high pressures.

As the pressure increases, while keeping the same inlet velocities, the simulated results show a decrease of heat transfer from the hot wall to the tube center due to radiation transport. This effect is due to an increase of the CO_2 optical thickness which contributes to stop the radiation transport from the hot wall to the colder fluid at the pipe center. Thus, as the pressure increases one can consider that radiative exchanges between CO_2 and the wall occur more gradually, the radiation from the wall heats only the fluid in its own vicinity as does CO_2 which exchanges by radiation only with its close neighborhood. As the pressure increases (e.g. above 5 Mpa), the pure CO_2 media become optically thick and one can model the radiation transport by a diffusion process and use simple radiative models such as the diffusion approximation (P_1 model) or the Rosseland approximation [14]. Moreover, the presented results clearly show the radiative transfer can be neglected in pure CO_2 above 20 MPa. It is worth noting that these results do not stand for an accurate determination of pressure intervals where a given model can be used, but they show the trend associated to the influence of pressure on radiation transport in a high temperature pipe.

6. Conclusion

A two-dimensional axisymmetric model to solve the turbulent flow and the heat transfer inside a hot pipe is described. The pipe temperature is assumed constant at 1100 K and CO_2 inlet temperature is 400 K. The influence of radiation on the flow temperature and velocity distribution is discussed. It is shown that the influence of radiation is important at low pressure (less than 5 MPa) but becomes negligible at pressure larger than 5 MPa. In the pressure range 0.1-5 MPa radiation results in CO_2 flow temperature and velocity increases. The influence of radiation on both temperature and velocity decreases with an increase of the working pressure and becomes non significant at about 20 MPa. This means that the influence of radiation absorption is rather weak at high pressure for the optical thickness involved in this study. At high pressure CO_2 becomes optically thick and radiation is absorbed in the very thin layer near the hot wall. Consequently, this shadowing effect limits drastically radiation propagation through the pipe.

Acknowledgements

The authors want to thanks Pr. Jean-Michel Hartmann for his valuable advices concerning high pressure radiative properties of CO_2.

REFERENCES

1. Y. Chen, W. Pridasawas and P. Lundqvist, *Dynamic simulation of a solar driven carbon dioxide transcritical power system for small scale combined heat and power production*, Solar Energy, **84** (2010), 1103–1110.
2. H. Chen, Y. Goswami and Stefanakos E., *A review of thermodynamic cycles and working fluid for the conversion of low grade heat*, Renewable and Sustainable Energy Reviews, **14** (2010), 3059–3067.

3. H. Yamaguchi, X.R. Zhang, K. Fujima, M. Enomoto and N. Sawada, *A solar energy powered Rankine cycle using supercritical carbon dioxide*, Applied Thermal Engineering, **26** (2006), 2345–2354.
4. X.R. Zhang , H. Yamagushi, and D. Uneno, *Experimental study of the performance of solar Rankine system using supercritical CO_2*, Renewable Energy, **32** (2007), 2617–2628.
5. V. Dostal, "A supercritical carbon dioxide cycle for next generation nuclear reactors," PhD thesis, Department of Nuclear Engineering, MIT, 2004. Available from: http://dspace.mit.edu/handle/1721.1/17746.
6. S.A. Wright, R.F. Radel, M.E. Vernon, G.E. Rochau, and P.S. Pickard, *Operation and analysis of a supercritical CO_2 brayton cycle*, Technical Report, Sandia Report SAND2010-0171, Sandia National Laboratories, 2010. Available from: http://prod.sandia.gov/techlib/access-control.cgi/2010/100171.pdf.
7. J.-E. Cha, T.-H. Lee, J.-H. Eoh, S.-H. Seong, S.-O Kim, D.-E. Kim, M. Kim, T.-W. Kim, and K.-Y. Suh, *Development of a supercritical CO_2 brayton energy conversion system coupled with a sodium cooled fast reactor*, Nuclear Engineering and Technology, **41** (2009), 1025–1044.
8. R.Z. Litwin, A.J. Zillmer, N.J. Hoffman, A.V. von Arx, and D. Wait, *Supercritical CO_2 turbine for use in solar power plants*, United States Patent US 7685820B2, 2010.
9. J. Liu, H. Chen, Y. Xu, L. Wang, C. Tan, *A solar energy storage and power generation system based on supercritical carbon dioxide*, Renewable Energy, **64** (2014), 43–51.
10. G. Turchi G., Z. Ma, T.W. Neises, M.J. Wagner, *Thermodynamic study of advanced supercritical carbon dioxide cycles for concentrated solar power*, ASME Journal of Solar Energy Engineering, **135** (2013), 041007–041013.
11. X.D. Niu, H. Yamaguchi, X.R. Zhang, Y. Iwamoto and N. Hashitani , *Experimental study of heat transfer characteristics of supercritical CO2 fluid in collectors of solar Rankine cycle system*, Applied Thermal Engineering, **31** (2011), 1279–1285.
12. H.Y. Kim, H. Kim, J.H. Song, B.H. Cho and Y.Y. Bae, *Heat transfer test in a vertical tube using CO2 at supercritical pressures*, Journal of Nuclear Science and Technology, **44** (2007), 285–293.
13. R. Span and W. Wagner, *A new equation of state for carbon dioxide covering the fluid region from the triple-point temperature to 1100 K at pressures up to 800 MPa*, Journal of Physical and Chemical Reference Data, **25** (1996), 1509–1596.
14. M.F. Modest, *Radiative heat transfer*. McGraw-Hill, New York, 1993.
15. G.D. Raithby and E.H. Chui, *A finite-volume method for predicting a radiant heat transfer in enclosures with participating media*, ASME Journal of Heat Transfer, **112** (1990), 415–423.
16. J. Taine and A. Soufiani, *Gas IR radiative properties: From spectroscopic data to approximate models*, Advances in Heat Transfer, **33** (1999), 295–414.
17. L.S. Rothman, I.E. Gordon, R.J. Barber, H. Dothe, R.R. Gamache, A. Goldman, V.I. Perevalov, S.A. Tashkun, and J. Tennyson, *HITEMP, the high-temperature molecular spectroscopic database*, Journal of Quantitative Spectroscopy and Radiative Transfer, **111** (2010), 2139–2150.
18. S.A. Tashkun and V.I. Perevalov, *CDSD-4000: High-resolution, high-temperature carbon dioxide spectroscopic databank*, Journal of Quantitative Spectroscopy and Radiative Transfer, **112** (2011), 1403–1410.
19. J.-M. Hartmann, C. Boulet, and D. Robert, *Collisional effects on molecular spectra: Laboratory experiments and models, consequences for applications*, Elsevier Sciene Ltd, 2008.
20. C. Caliot, Y. Le Maoult, M. El Hafi, and G. Flamant, *Remote sensing of high temperature H_2O-CO_2-CO mixture with a correlated k-distribution fictitious gas method and the single-mixture gas assumption*, Journal of Quantitative Spectroscopy and Radiative Transfer, **102** (2006), 304–315.
21. M.Y. Perrin and J.M. Hartmann, *Temperature-dependent measurements and modeling of absorption by CO_2-N_2 mixtures in the far line-wings of the 4.3[mu]m CO_2 band*, Journal of Quantitative Spectroscopy and Radiative Transfer, **42** (1989), 311–317.

22. S.V. Patankar and B.D. Spalding, *A calculation procedure for heat, mass and momentum transfer in three-dimensional parabolic flows*, International Journal of Heat and Mass Transfer, **15** (1972), 1787–1806.

23. B.P. Leonard and S. Mokhtari, *ULTRA-SHARP nonoscillatory convection schemes for high-speed steady multidimensional flow*, Technical Memorandum 102568 (ICOMP-90-12), NASA Lewis Research Center, 1990.

24. B. Kader, *Temperature and concentration profiles in fully turbulent boundary layers*, International Journal of Heat and Mass Transfer, **24** (1981), 1541–1544.